Fast and slow gating are inherent properties of the pore module of the K^+ channel Kcv

Alessandra Abenavoli,[1] Mattia Lorenzo DiFrancesco,[1] Indra Schroeder,[2] Svetlana Epimashko,[1] Sabrina Gazzarrini,[1] Ulf Peter Hansen,[2] Gerhard Thiel,[3] and Anna Moroni[1]

[1]Dipartimento di Biologia and Istituto di Biofisica-Consiglio Nazionale delle Ricerche, Università degli Studi di Milano, 20133 Milan, Italy
[2]Department of Structural Biology, University of Kiel, 24098 Kiel, Germany
[3]Institute of Botany, Darmstadt University of Technology, 64287 Darmstadt, Germany

Kcv from the chlorella virus PBCV-1 is a viral protein that forms a tetrameric, functional K^+ channel in heterologous systems. Kcv can serve as a model system to study and manipulate basic properties of the K^+ channel pore because its minimalistic structure (94 amino acids) produces basic features of ion channels, such as selectivity, gating, and sensitivity to blockers. We present a characterization of Kcv properties at the single-channel level. In symmetric 100 mM K^+, single-channel conductance is 114 ± 11 pS. Two different voltage-dependent mechanisms are responsible for the gating of Kcv. "Fast" gating, analyzed by β distributions, is responsible for the negative slope conductance in the single-channel current–voltage curve at extreme potentials, like in MaxiK potassium channels, and can be explained by depletion-aggravated instability of the filter region. The presence of a "slow" gating is revealed by the very low (in the order of 1–4%) mean open probability that is voltage dependent and underlies the time-dependent component of the macroscopic current.

The Journal of General Physiology

INTRODUCTION

The K^+ channel Kcv from the chlorella virus PBCV-1 (Plugge et al., 2000) is a miniature potassium channel, with only 94 amino acids. By homology with the already known crystal structures of similar bacterial channels, and in particular with that of KirBac1.1 (Kuo et al., 2003), the monomer of Kcv is assumed to be formed by two transmembrane (TM) domains (TM1 and TM2), the filter region bearing the consensus sequence (TxxTxGY/FGD), an extracellular turret, and a very short (12 amino acids) N-terminal domain that forms a short slide helix (Tayefeh et al., 2007). The channel ends with TM2, and the C terminus resides presumably within the membrane thickness. For its extremely reduced dimensions, Kcv represents a very simple and primitive K^+ channel. Therefore, the electrical properties of Kcv are of fundamental interest to perform structure–function studies. At the moment, Kcv has been extensively characterized in whole cell experiments by heterologous expression in *Xenopus* oocytes or HEK 293 cells (Gazzarrini et al., 2002; Moroni et al., 2002). Single-channel measurements were so far obtained only in artificial membrane bilayer (Pagliuca et al., 2007; Shim et al., 2007).

Two-electrode voltage clamp recordings in *Xenopus* oocytes have revealed a characteristic shape of the Kcv open-channel I-V relationship (including a negative slope conductance at extreme potentials) and kinetics of activation at negative potentials (Gazzarrini et al., 2002). These observations can be related either to voltage-dependent gating mechanisms or to changes in conductance. To confirm that these properties are in fact due to gating mechanisms, single-channel measurements in the same expression system became necessary for the reconstruction of macro-currents from single-channel properties.

Here, we describe the properties of Kcv single-channel currents in *Xenopus* oocytes to examine their gating characteristics. We show that Kcv, despite its small dimensions, is clearly gated. In particular, a fast- and a slow-gating mechanism are both acting in a voltage-dependent way. The presence of gating mechanisms in Kcv is of great significance. In fact, it shows that a simple pore domain, without long cytosolic regions and probably with no bundle crossing (Tayefeh et al., 2009), can open and close in response to voltage. This supports the growing evidence of a gating mechanism at the level of the selectivity filter in other K^+ channels (Liu et al., 1996; VanDongen, 2004; Bernèche and Roux, 2005; Schroeder and Hansen, 2007).

A. Abenavoli and M.L. DiFrancesco contributed equally to this work.
Correspondence to Anna Moroni: anna.moroni@unimi.it
Abbreviation used in this paper: TM, transmembrane.

© 2009 Abenavoli et al. This article is distributed under the terms of an Attribution–Noncommercial–Share Alike–No Mirror Sites license for the first six months after the publication date (see http://www.jgp.org/misc/terms.shtml). After six months it is available under a Creative Commons License (Attribution–Noncommercial–Share Alike 3.0 Unported license, as described at http://creativecommons.org/licenses/by-nc-sa/3.0/).

The Rockefeller University Press $30.00
J. Gen. Physiol. Vol. 134 No. 3 219–229
www.jgp.org/cgi/doi/10.1085/jgp.200910266

MATERIALS AND METHODS

Oocyte expression

Capped PBCV-1 Kcv cRNAs were prepared as described by Plugge et al. (2000). In brief, *kcv* cDNA was cloned into pSGEM vector (a modified version of pGEM-HE; provided by M. Hollmann, Max Planck Institute for Experimental Medicine, Gottingen, Germany). cRNA was transcribed in vitro using T7 RNA polymerase (Promega) and injected (50 ng/oocyte) into *Xenopus laevis* oocytes, prepared according to standard methods (Plugge et al., 2000). Oocytes were incubated at 19°C in ND96 solution (96 mM NaCl, 2 mM KCl, 1.8 mM $CaCl_2$, 1 mM $MgCl_2$, and 5 mM HEPES, adjusted to pH 7.5 with NaOH). The experiments were performed 2–7 d after injection.

Electrophysiology

Expression was monitored by recording currents in two-electrode voltage clamp configuration (Geneclamp 500; MDS Analytical Technologies). Electrodes were filled with 3 M KCl and had a resistance of 0.4–0.8 MΩ in 50 mM KCl. The oocytes were perfused at room temperature with a standard bath solution containing 50 mM KCl, 1.8 mM $CaCl_2$, 1 mM $MgCl_2$, and 5 mM HEPES, with pH adjusted to 7.4 with KOH and osmolarity to 215 mOsm with mannitol. Oocytes showing >6 μA of current at $V = 60$ mV were used for patch clamp experiments. Patch pipettes were pulled from thin-walled borosilicate glass capillaries, coated with Sylgard (Corning), and fire-polished to a final resistance of 0.8–1 MΩ for macro-currents and 8–15 MΩ for single-channel experiments. Standard pipette solution contained 100 mM KCl, 1.8 mM $CaCl_2$, 1 mM $MgCl_2$, and 10 mM HEPES, pH to 7.4 with KOH. Macro-currents and single-channel recordings were made in cell-attached and inside-out configurations. The standard bath solution contained 100 mM KCl, 1 mM $MgCl_2$, 1 mM EGTA, and 10 mM HEPES, pH to 7.4 with KOH. Experiments were performed at room temperature after removal of the vitelline membrane from oocytes in a hyperosmotic solution (ND96 solution plus 100 mM NaCl). Currents were recorded with a Dagan 3900 amplifier, and data were low-pass filtered at 1 kHz and digitized at a sampling rate of 10 kHz for macro-currents. For single-channel recordings, the four-pole Bessel filter was set to 2–5 kHz and the sampling rate to 10–25 kHz. Different solutions were fed by gravity, and solution change took no more than 20 s. Single-channel analysis was done using pCLAMP 9 (MDS Analytical Technologies) with the threshold-based algorithm, except for fast-gating analysis (see below).

Evaluation of fast gating

The measured current in the open state of the channel displays increased noise if gating is faster than can be resolved by the recording apparatus. Often, the value of the apparent single-channel current, I_{app}, extracted from such records is smaller than the value of the true single-channel current, I_{true} (which would be measured if the temporal resolution of the recording apparatus were high enough). Both I_{true} and I_{app} require clear adequate algorithms as a basis for their determinations from measured time series (Hansen et al., 2003; Schroeder and Hansen, 2006, 2007, 2008). Base line drift, membrane flickering, endogenous channels, and other artifacts would distort the analysis. Thus, all data had to be closely inspected and cleaned manually from sections showing these kinds of artifacts (Sigworth, 1985). Sections of fast gating were extracted from the measured time series (excluding sections of obviously closed states) by means of a Hinkley detector in the program Kiel-Patch (Schultze and Draber, 1993). These "cleaned time series" were used to generate the open-point histogram (distribution-per-level; Schröder et al., 2004) of the apparent open state.

Determination of the apparent single-channel current, I_{app}

The apparent current I_{app} as obtained from the maximum of the amplitude histograms strongly depends on the corner frequency of the filter of the recording setup (Fig. 2 in Schroeder and Hansen, 2008). Nevertheless, it can reach a well-defined asymptotic value when the corner frequency of the electronic filter is low enough. This value is used here because it corresponds to the instantaneous current level obtained from whole cell recordings. Because the cleaned time series comprise only sections of fast gating, they constitute a stationary time series of great length, thus enabling the application of filtering (moving average in Kiel-Patch) of sufficient low frequency (mainly 500 Hz) and the determination of the asymptotic value of I_{app}.

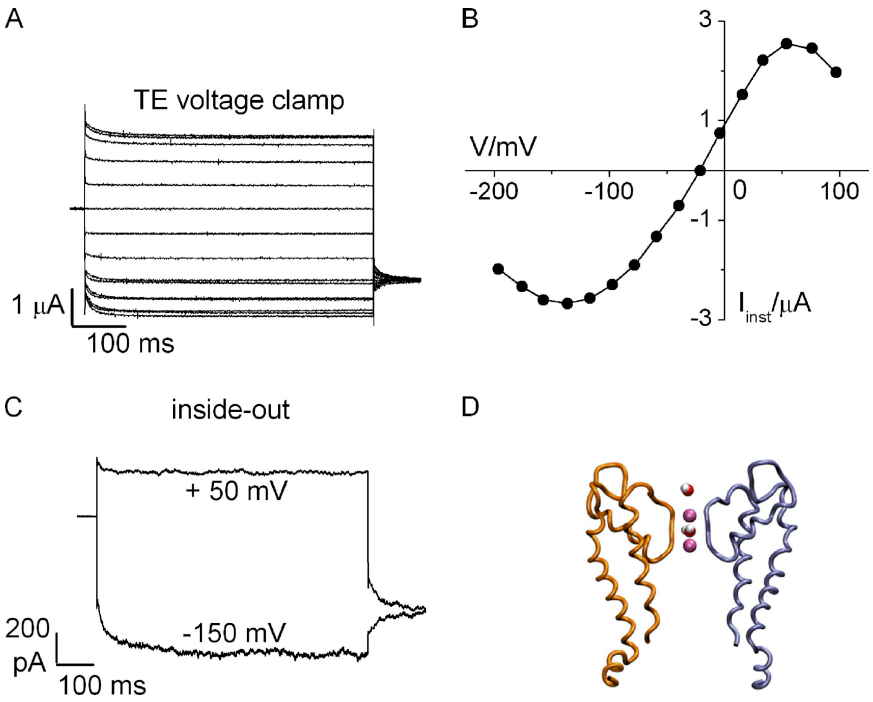

Figure 1. Kcv macro-currents recorded in *Xenopus* oocytes. (A) Currents recorded by two-electrode (TE) voltage clamp from a holding potential of −20 mV, followed by steps of 20 mV ranging between 100 and −200 mV, and returning at −80 mV. Bath solution: 50 mM KCl, 1.8 mM $CaCl_2$, 1 mM $MgCl_2$, and 5 mM HEPES, pH 7.5. Osmolarity was adjusted to 215 mOsm with mannitol. (B) I-V curve of the instantaneous current shown in A. (C) Currents recorded from macropatch in inside-out configuration. Holding potential of 0 mV, with steps +50 and −150 mV, returning at −80 mV. Pipette solution: 100 mM KCl, 1.8 mM $CaCl_2$, 1 mM $MgCl_2$, and 10 mM HEPES/pH 7.3. Bath solution: 100 mM KCl, 1 mM $MgCl_2$, 1 mM EGTA, and 10 mM HEPES/pH 7.3. (D) Putative structure of Kcv showing in orange and blue two of the four identical subunits of the tetrameric channel. The figure illustrates a snapshot of a molecular dynamics simulation of the Kcv model (Tayefeh et al. 2009).

The experiments in MaxiK were done in HEK293 cells with a filter corner frequency of 50 kHz, whereas a 5-kHz filter was used here for Kcv. To test whether the different experimental conditions may have an influence, the data of MaxiK (Schroeder and Hansen, 2007) were refiltered by a digital 5-kHz four-pole Bessel filter. The refiltered data led to the same results as the 50-kHz data (not depicted). This indicates that differences in the behavior of Kcv and MaxiK are not caused by the different temporal resolution of measurements in Kcv and MaxiK.

Determination of the true single-channel current, I_{true}, and of the rate constants of an O-C model of fast gating

The open-state amplitude histogram of I_{app} as obtained from the bursts is broader than that of the base line, and its curve shape may deviate from that of a Gaussian distribution (Fitzhugh, 1983; Yellen, 1984; Klieber and Gradmann, 1993) (see Fig. 4 A). These so-called β distributions can be used to determine the true single-channel current and the rate constants of the underlying Markov model (Schroeder and Hansen, 2006, 2007, 2008). Schroeder and Hansen (2006) have shown that it is sufficient to use a truncated Markov model (two states: O-C) for the analysis of the bursts in the time series.

A simplex algorithm (Caceci and Cacheris, 1984) was used to fit the "theoretical" open-point histogram obtained from the two-state model to the open-point histogram of the measured data. Unfortunately, there is no straightforward procedure to calculate β distributions obtained from higher-order filters (Riessner, 1998). Thus, simulations instead of deterministic algorithms were used to provide the theoretical curves. This is quite time-consuming during a fitting routine, but it turned out to be the most efficient way to resolve fast flickering.

The fit algorithm has to determine three parameters of the O-C model: the true open-channel current I_{true} and the rate constants k_{OC} and k_{CO}. Even though it provides the automatic determination of all three parameters (Schroeder and Hansen, 2006), the fitting procedure treated I_{true} and k_{CO} and k_{OC} differently. The current was used as a fixed parameter that was changed stepwise in subsequent fits. The computer determined the best set of k_{OC} and k_{CO} for each suggested current. The resulting plot "error sum versus assumed I_{true}" was very helpful for the estimation of the reliability of the fit (see Fig. 4 B). In the case of good data, a pronounced minimum was found, and the location of this minimum was taken as the true single-channel current (see Fig. 4 B). The rate constants k_{CO} and k_{OC} of the related fit were used for Fig. 5 B. The software for Kiel-Patch and for the β fits (downhill) is available at www.zbm.uni-kiel.de/aghansen/software.html.

RESULTS

Macroscopic currents

Compared with K^+ channels from pro- and eukaryotes, the viral channel Kcv is small indeed (Plugge et al., 2000). The homology model generated with the prokaryotic channel KirBac1.1 (Tayefeh et al., 2009) shows that Kcv represents the pore module (TM1–pore loop–TM2) of K^+ channels (Fig. 1 D). But in spite of this simple structure, the macroscopic conductance of Kcv still shows interesting gating features and voltage-dependent properties: two-electrode voltage clamp recordings of the channel in *Xenopus* oocytes reveal two kinetic components comprising an instantaneous and a time-dependent conductance (Fig. 1 A). The time-dependent component is superimposed on the instantaneous component and activates at negative voltages and deactivates at positive voltages in a voltage-dependent manner. The instantaneous

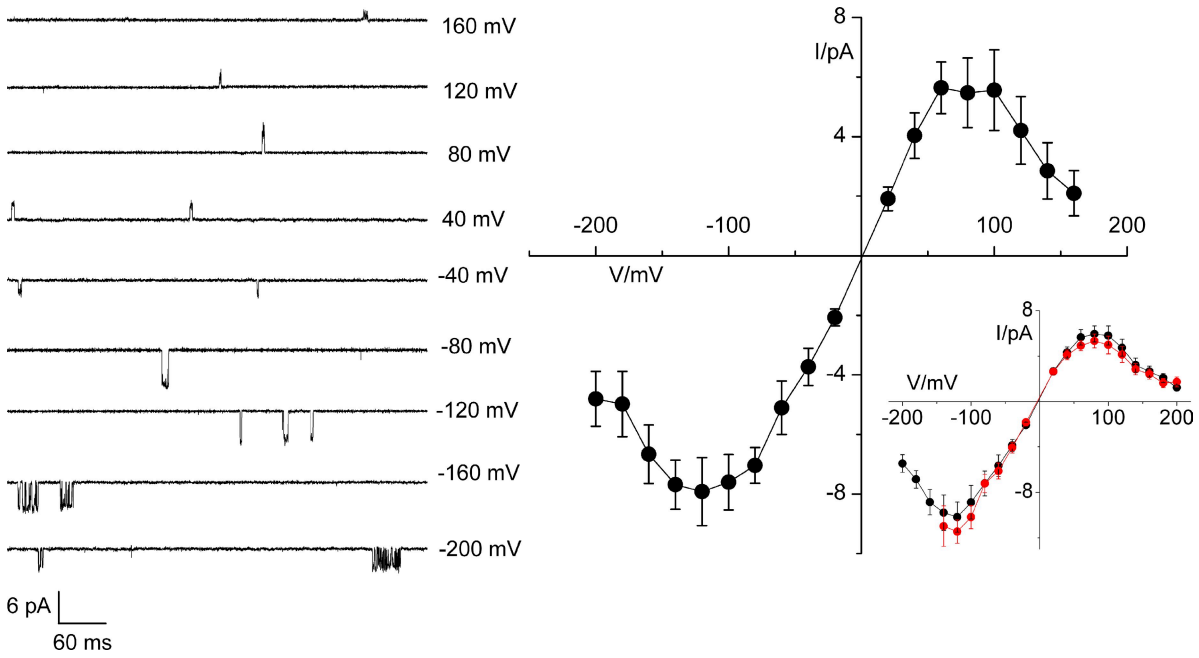

Figure 2. Single-channel recordings obtained from Kcv expressed in oocytes. (Left) Time series measured in the cell-attached mode at different potentials as indicated. Pipette solution contained (in mM): 100 KCl, 1.8 $CaCl_2$, 1 $MgCl_2$, and 10 HEPES, pH 7.3. (Right) Single-channel I-V curve of the experiment on the left. (Inset) Comparison of experiments performed in cell-attached (black symbols) and inside-out mode (red symbols) in the following bath solution (in mM): 100 KCl and 1 HEPES, pH 7.3. Mean values ± SD, unitary channel openings from two independent experiments; $n \geq 300$ apart from the value at −140 mV in inside-out, in which $n = 8$.

current is quasi-linear in a voltage window of ±40 mV around the reversal potential (Fig. 1 B). At more extreme clamp voltages, the current shows a negative slope conductance. In inside-out configuration, the macro currents show the same characteristic voltage-dependent kinetics of activation and inactivation (Fig. 1 C). To understand if kinetics and voltage dependence are inherent gating features of the channel, we have characterized Kcv at the single-channel level, as reported below.

Single-channel recordings

To allow the desired direct comparison between microscopic and macroscopic currents, we measured the single-channel activity in *Xenopus* oocytes. Unitary channel fluctuations of Kcv have been recorded in the cell-attached configuration over a wide voltage range. Fig. 2, left shows typical current traces with apparently one Kcv channel in the patch.

The single-channel current reveals characteristic features: at moderate voltages the channel opens to well-defined open levels, whereas at high negative and positive potentials the apparent conductance decreases and the openings become noisy (see Fig. 3). This leads to the mean apparent single-channel I-V relation of Kcv shown in Fig. 2, right that fully reproduces the nonlinear behavior of the macroscopic I-V relation (Fig. 1 B). The curve is quasi-linear in a voltage range between −40 and +40 mV. At more positive and more negative voltages, the I-V relation shows a negative slope. In its linear part (±40 mV), we estimated a conductance of $g = 114 \pm 11$ pS ($n = 10$). This value and the general shape of the I-V relationship are in agreement with those estimated for Kcv in planar lipid bilayers under the same ionic conditions (Pagliuca et al., 2007; Shim et al., 2007).

All I-V curves reversed around 0 mV, as expected for a selective K^+ channel in symmetric KCl conditions (considering the internal K^+ concentration in oocytes is ∼100 mM; Weber, 1999). The same I-V relation was obtained in inside-out configuration (Fig. 2, right, inset) when all possible sources of channel block had been removed from the solution (magnesium and chelators) or lowered 10 times (HEPES). The apparent decrease in conductance at extreme potentials (Figs. 1 B and 2, right) and the accompanying increase in noise (Fig. 2, left) are always observed and can be considered characteristic of Kcv, but the polarity of the voltage effect is not constant. Fig. 3 compares two different behaviors observed in Kcv. Fig. 3 (left) shows an experiment where the reduction of apparent current, as a consequence of flickering at extreme potentials, is more pronounced at positive than at negative voltages (compare for instance apparent current at +140 and −140 mV). Fig. 3 (right) shows another experiment in which current reduction at extreme voltages is opposite from Fig. 3 (left), more marked at negative than at positive voltages. The most common behavior found is that of Fig. 3 (left), supporting the choice of data shown in Fig. 2, left. But we also found the opposite behavior, shown in Fig. 3 (right). Different behaviors are usually found in different batches of oocytes, although once they were found in the same oocyte. Similar observations have been reported for Kcv single-channel measurements in artificial lipid bilayer (Pagliuca et al., 2007). In this case, the mirror image of Kcv was interpreted as evidence of two possible orientations of the inserted protein.

Analysis of fast gating

Negative slopes in apparent single-channel I-V curves (Fig. 2, right) are often caused by unresolved fast gating or "flickering" (Klieber and Gradmann, 1993; Draber and Hansen, 1994; Schroeder and Hansen, 2006, 2007, 2008). Here, the involvement of flickering is suggested by the increased open-channel noise at extreme potentials (Figs. 2 and 3) (Sigworth, 1985; Hille, 1992; Townsend and Horn, 1999). The most powerful method of looking at gating effects beyond the corner frequency of the experimental setup (2 or 5 kHz) is based on the analysis of amplitude histograms by means of β distributions

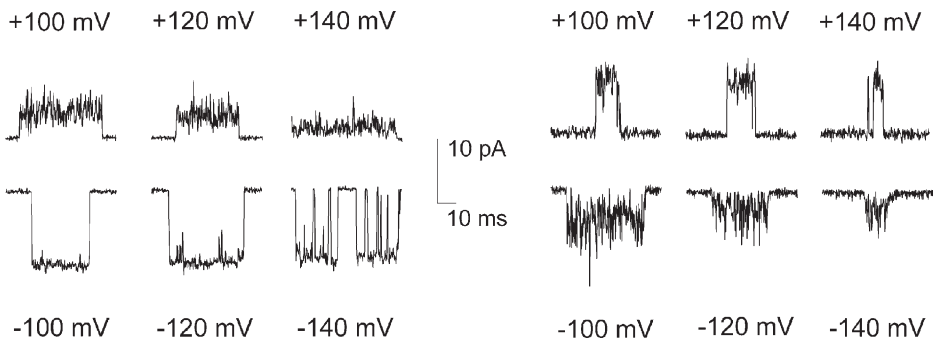

Figure 3. Voltage-dependent behavior of the apparent conductance in Kcv. Comparison of bursts obtained at ±100, ±120, and ±140 mV (top traces, positive potentials; bottom traces, negative potentials) from two different experiments. (Left) In this experiment, the decrease in conductance and the increase in noise are more marked at positive than at negative voltages. (Right) Opposite dependence on voltage of current reduction found in a different experiment. In this experiment, the decrease in apparent conductance and the increase in open-channel noise are more evident at negative than at positive potentials.

(Heinemann and Sigworth, 1991; Weise and Gradmann, 2000; Schroeder and Hansen, 2006, 2007, 2008). Analysis by β distributions of currents recorded in cell-attached mode at +80 mV is illustrated in Fig. 4. In brief (see Materials and methods for further details), closed-channel (Fig. 4 A, black line) and open-channel (red line) point distributions are generated. A truncated Markov model (two states: O-C) with fixed I_{true} was used to simulate a time series. The open-level distribution of the simulated time series is fitted to the measured distribution by minimization of the error sum to find the best pair of rate constants (Schroeder and Hansen, 2007). Repeating the fitting routine with different values of I_{true} led to different error sums: the minimum in the error sum curve (Fig. 4 B) is assumed to mark the true current. The green line in Fig. 4 A is the simulated open-point distribution with I_{true} obtained with this procedure.

Fig. 5 A shows the I-V curve of I_{true} as compared with I_{app}, and in Fig. 5 B, the related rate constants are presented. According to the results in Fig. 5 A, the true single-channel current does not show a negative slope at positive potentials; instead, moderate saturation is present. This indicates that the negative slope of the apparent current is caused by fast gating. The gating frequencies related to time constants in the range of 1 to 100 µs (Fig. 5 B) are too fast as compared with the filter corner frequency of 2 or 5 kHz. Thus, I_{app} is presented as an average over closed and open times at the output of the patch clamp amplifier.

Comparison of these results for Kcv with previous fast-gating analysis on MaxiK (Schroeder and Hansen, 2007) reveals that the similar tendency of current reduction at positive potentials is due to fast closure of the channel. The rate constants of gating of Fig. 5 B show an increase in the value of k_{OC} at positive potentials, suggesting that fast gating is caused by an increased instability of the open state. Kcv shows strong voltage dependence in k_{CO}, which decreases monotonically with depolarizing potentials (Fig. 5 B) and a somewhat parabolic dependence on membrane potential in k_{OC} (Fig. 5 B). Because of the symmetric behavior of k_{OC}, negative slopes of the apparent I-V curves are expected to occur on either side. However, the monotonous voltage dependence of k_{CO} partially compensates the changes of k_{OC} on the negative side. Because of this, negative slopes at negative membrane potentials are found at higher absolute voltages in Kcv than at the positive side. Gating analysis by β distributions in this region was impeded by two effects: the rare occurrence of records and their noisiness. After having done the analysis of fast gating, the so-called gating factor R (i.e., the ratio R of true [I_{true}] and apparent current [I_{app}]; Eq. 1) can be calculated in two different ways (Schroeder and Hansen, 2007). It can be obtained from the average of the current in the burst of the time series (Fig. 2, left),

$$R_I = \frac{I_{true}}{I_{app}}, \tag{1}$$

or from the parameters of the two-state model of gating (Fig. 5 B),

$$R_K = \frac{k_{CO} + k_{OC}}{k_{CO}}. \tag{2}$$

In Fig. 5 C, R obtained either way is displayed for Kcv. The coincidence of both curves is a sign of the reliability of the analysis. The voltage dependence of the gating factor reveals a strong increase at high positive potentials. This resembles the situation as found in MaxiK channels (Schroeder and Hansen, 2007). The increase of the gating factor at positive potentials can be fitted by an exponential function of membrane voltage V:

$$R = \frac{I_{true}}{I_{app}} = R_0 + R_K \exp\left(\frac{V}{V_G}\right), \tag{3}$$

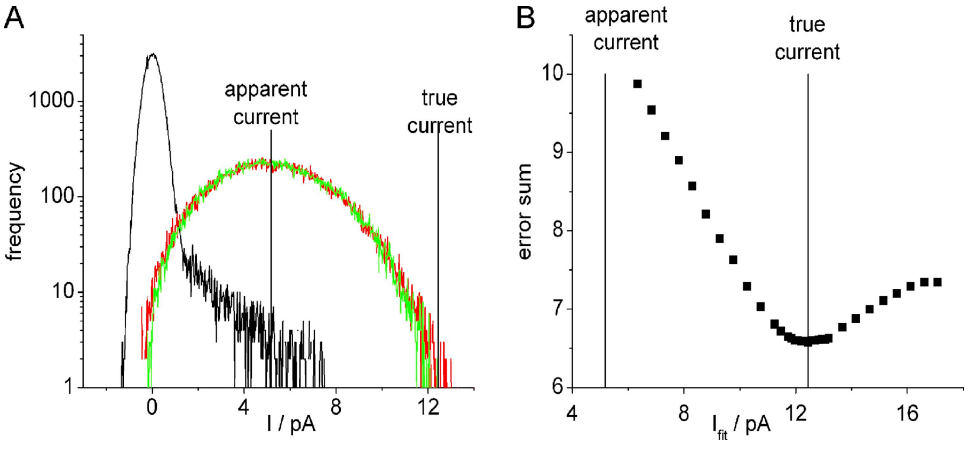

Figure 4. Analysis performed by β distributions. (A) Point amplitude distributions from a time series recorded at +80 mV are shown (black line, close level; red line, open level). I_{app} = 5.17 pA (vertical line) is obtained from the maximum of the open-point amplitude histogram (red line). The green line is the open-point amplitude distribution obtained from the time series simulated by an O-C model and fitted to the measured distribution (red line). This procedure gives the best pairs of rate constants (k_{OC} = 58,400 s^{-1} and k_{CO} = 42,200 s^{-1} for the example shown). For each simulation, the current I was used as a fixed parameter and was changed stepwise in subsequent fits. The current value that gives the minimum value in the error sum (see B) is defined as I_{true} (vertical line). (B) Dependence of the error sum of the fit on the assumed value of I. I_{true} = 12.5 pA (vertical line) is the value of I that gives the minimum value in the error sum in this example.

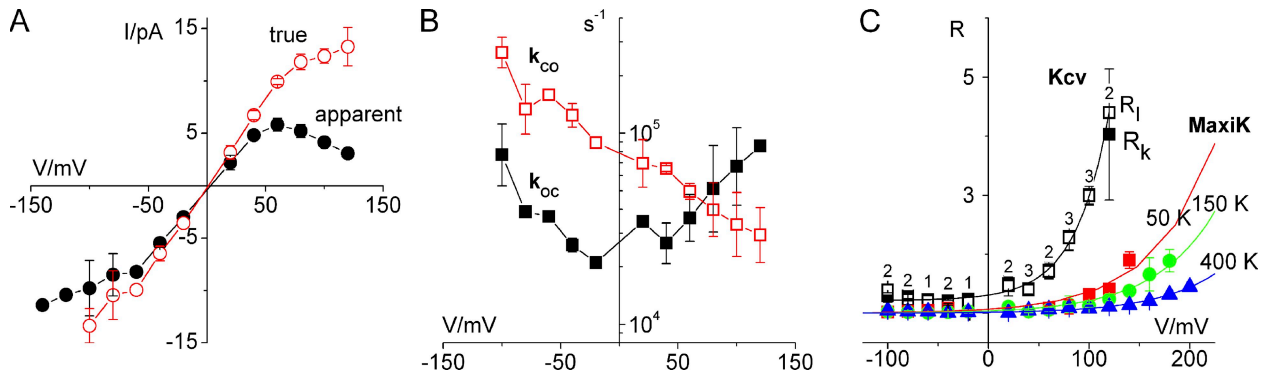

Figure 5. Voltage dependence of fast gating. (A) I-V curves of I_{app} (filled black circles) obtained from the time series directly by averaging over the bursts, and I_{true} (open red circles) evaluated from the β distribution fits. (B) Voltage dependence of k_{OC} (filled black squares) and k_{CO} (open red squares). (C) The gating factor R obtained from Kcv at 100 mM KCl and from MaxiK obtained at 50, 150, and 400 mM KCl. For Kcv, R_I and R_K are both displayed (open squares and filled squares, respectively); for MaxiK, only R_I is displayed. The smooth lines approximating the data points present the exponential fits by means of Eq. 3. Parameters for Kcv: $R_0 = 1.2 \pm 0.1$ mV, $V_G = 34 \pm 3$ mV, and $R_K = 11 \pm 3$. Numbers of individual experiments are given for Kcv.

with $R_O = 1.2$ being the offset, $R_K = 0.9$ the amplitude factor of the exponential term, and $V_G = 34$ mV the characteristic voltage. V_G in MaxiK (60 mV) was twice as much as in Kcv (34 mV). This indicates that gating in Kcv is more voltage dependent than in MaxiK.

The key for the assignment of fast gating in MaxiK to a depletion-induced instability of the selectivity filter was the dependence on the concentration of the permeant ion (Fig. 5 C). We therefore tested the effect of increasing the K^+ concentration on outward and inward Kcv currents. Fig. 6 A shows current values recorded from the same patch in cell-attached (K^+_{in}, ∼100 mM; black line) and inside-out mode (K^+_{in}, 300 mM; red line), with 100 mM K^+ in the pipette (K^+_{out}). Interestingly, high (cytoplasmic) K^+ prevents reduction of current (Fig. 6 A) and conductance (Fig. 6 B), as observed in low K^+ at increasing positive voltages. Fig. 6 C compares traces recorded in low and high K^+ at approximately the same driving force (∼+80 mV from the calculated reversal potential). In high K^+, the current level is visibly higher than in low K^+. The enlarged traces in Fig. 6 C show that in high K^+, the single-channel openings can be less noisy (left) as expected. However, events with unreduced noise also still occur. This indicates that the attenuation of the ion-aggravated induced effect on the selectivity filter is less reproducible as it is in MaxiK (Schroeder and Hansen, 2007). As discussed below, this variability seems to be related to the minimal structure of Kcv. We interpret this finding as evidence that the tested K^+ concentration, 300 mM, is not yet saturating the effect on fast gating. Fig. 7 shows the effect of increasing K^+ concentrations on inward currents. Here, we compare two patches from the same oocyte recorded with 100 mM K_{out}^+ (Fig. 7, A and B, black line) and 300 mM K_{out}^+ (red line) in the pipette. High (extracellular) K^+ prevents current reduction at negative voltages (Fig. 7 A), as indicated by the single-channel conductance, constant over the voltage range (Fig. 7 B). Fig. 7 C shows that high K^+ reduces the noise and increases the current in single-channel events recorded at approximately the same driving force of those in low K^+ (∼−60 mV from the calculated reversal potential).

Slow gating: voltage-dependent open probability

The fast-gating behavior illustrated in Figs. 2 and 3 and analyzed in Figs. 4 and 5 contributes to the value of the instantaneous current I_{inst} in Fig. 1. Because the fast gating only results in a reduction of I_{true}, it is not responsible for the time-dependent component of the whole cell traces that is assumed to be related to the open probability of the single channel.

The steady-state open probability of Kcv is actually very variable all along single recordings and significantly low at each potential (<4%; see below). Two factors in particular render the analysis of open probability difficult: long periods of silence and the inestimable number of channels in the patch given the low open probability. These complications become obvious in the experiment of Fig. 8 A showing three extracts from a long record of 60 min at a constant holding potential of −60 mV. The NP_{open} calculated from subsequent 5-min-long sections increases dramatically during the recording (Fig. 8 B). This is probably due to the activation of some silent channels (as evident from double openings in Fig. 8 A, bottom trace), but seems to also entail an increase in the mean open probability of the single channel (also visible in Fig. 8 A, middle trace). For these reasons, we avoid the temptation to build up a comprehensive Markov model of Kcv including fast and slow gating.

To study the voltage dependence of open probability under these unfavorable conditions, we selected experiments with the lower value of open probability (1–4%). This behavior corresponds to that in the top trace of Fig. 8 A. To exclude outliers, we applied an additional constraint when selecting traces for the evaluation: the

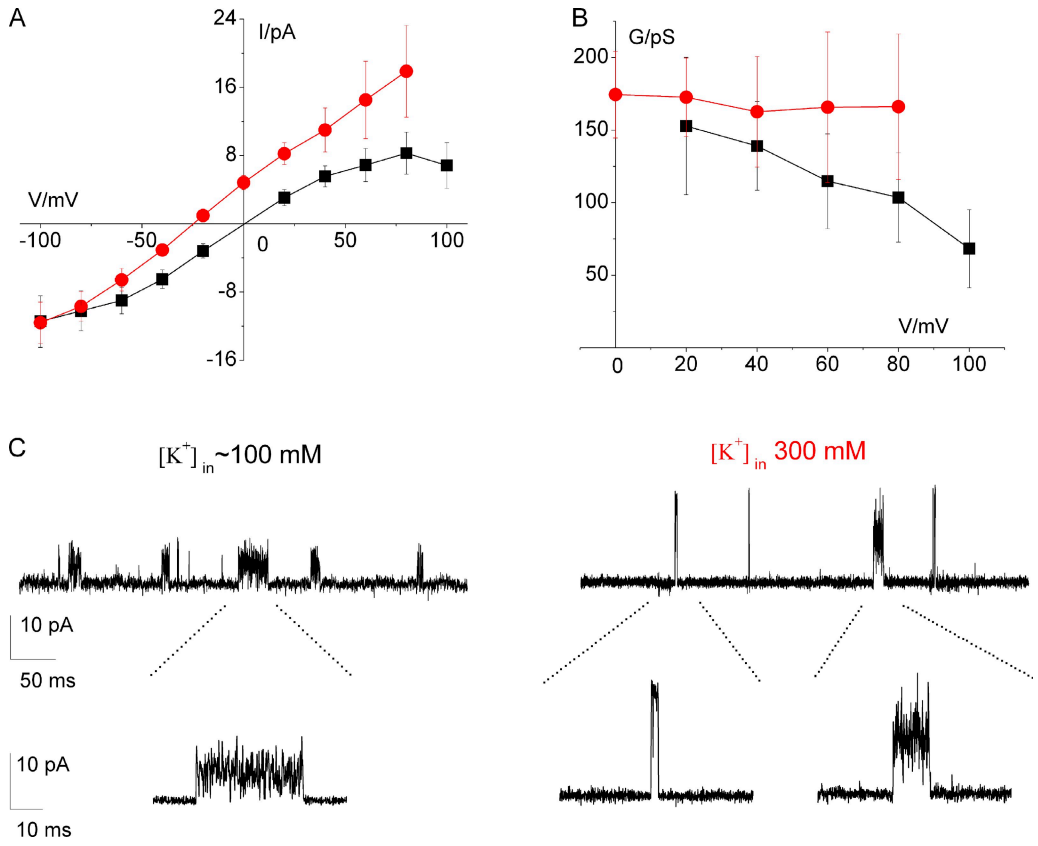

Figure 6. Effect of increasing $[K^+]_{in}$ on Kcv outward flickering. (A) Open-channel I-V relationship of Kcv recorded from the same patch in cell-attached configuration, $[K^+]_{in}$ = ~100 mM (black symbols and line), and in inside-out configuration, $[K^+]_{in}$ = 300 mM (red symbols and line). Pipette solution: 100 mM KCl, 1.8 mM $CaCl_2$, and 1 mM $MgCl_2$. Bath solution: 300 mM KCl, 1 mM EGTA, and 1 mM $MgCl_2$. (B) Voltage dependence of the calculated single-channel conductance (black, $[K^+]_{in}$ ~100 mM; red, $[K^+]_{in}$ 300 mM). (C) Comparison of single-channel fluctuations recorded in $[K^+]_{in}$ ~100 mM (left) and 300 mM (right) at about the same driving forces (~+80 mV from current reversal voltage). (Bottom) Enlargements of top traces.

variance of the open probability had to be equal for all membrane potentials. The last constraint was to ensure that the distribution of channel numbers was the same for all membrane potentials. The limitation of open probability may influence the determined voltage dependence. Nevertheless, if there were no voltage dependence, a horizontal dependence should be found. Fig. 8 C clearly shows that even under this restriction, a significant voltage dependence does occur. The voltage dependence is very weak (with a factor of 1.5/60 mV) even though it is statistically significant. The high scatter at negative potentials in Fig. 8 C also confirmed the variability of Kcv. By analyzing patches with higher open probability, we found a similar but stronger voltage dependence, increasing with negative voltages by a factor of 3/60 mV (not depicted). To correlate the open probability and the time-dependent component of macroscopic current, we used multichannel patch to reconstruct the macroscopic currents in Fig. 1 A by ensemble averaging. In the experiment of Fig. 8 D, the membrane was first clamped to +80 mV, a potential at which the channels were observed to be mostly nonconductive (NPo is lowest; Fig. 8 C), and then stepped to −100 mV for activation. The individual traces are already indicative of the voltage dependency, showing more activity at −100 than at +80 mV. The "whole cell" trace shown in the box of Fig. 8 D resulted from averaging over 100 different pulses. It reveals a clear slow activation at the negative voltage. This slow component can be fitted with a single exponential yielding a time constant of 17 ms. This value is in good agreement with the mean fast time constant obtained in two-electrode voltage clamp experiments (20 ± 4 ms; Gazzarrini et al., 2002).

DISCUSSION

The main result of this work is that two voltage-dependent gating processes are found in the minimal Kcv channel: a fast one in a time scale of microseconds and a slow one in a time scale of milliseconds. This indicates that the simple pore domain can gate. Another interesting point arises from the comparison of the results from Kcv and other channels, namely that an increase in complexity in protein structure, typical of mammalian

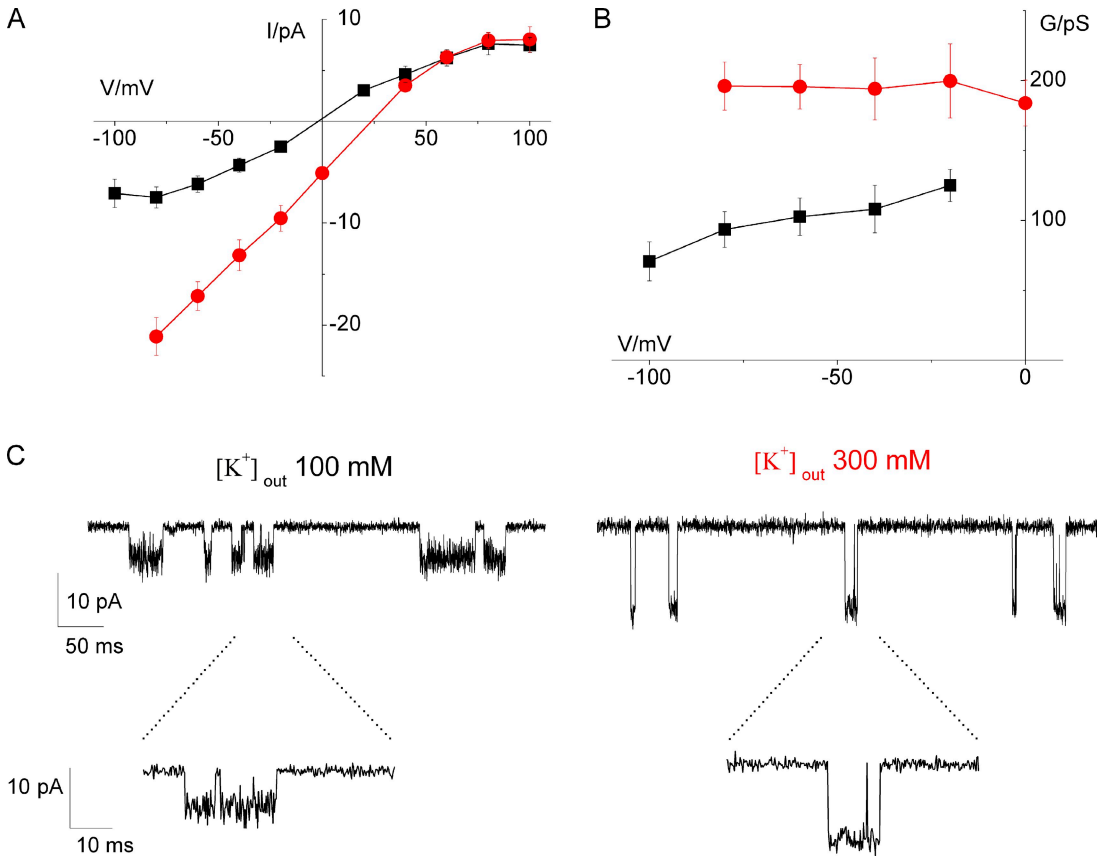

Figure 7. Effect of increasing $[K^+]_{out}$ on Kcv inward flickering. (A) Open-channel I-V relationships of Kcv recorded in cell-attached configuration in $[K^+]_{out}$ = 100 mM (black symbols and line) and $[K^+]_{out}$ = 300 mM (red symbols and line). Pipette solution: 100 or 300 mM KCl, 1.8 mM $CaCl_2$, and 1 mM $MgCl_2$. Bath solution: 100 mM KCl, 1 mM EGTA, and 1 mM $MgCl_2$. (B) Voltage dependence of the calculated single-channel (black, $[K^+]_{out}$ ~100 mM; red, $[K^+]_{out}$ 300 mM). (C) Comparison of single-channel fluctuations recorded in $[K^+]_{out}$ 100 mM (left) and 300 mM (right) at almost the same driving forces (~−60 mV from current reversal voltage). (Bottom) Enlargements of top traces.

channels, seems to enhance the reliability and fidelity of the process, as discussed below.

A preliminary analysis of the instantaneous I-V relation of Kcv has been performed before (Gazzarrini et al., 2006). There, a reaction kinetic model was suggested implying that the negative slopes in the I-V relationship can be explained by an auto-inhibition in the chord conductance. This model predicts effects similar to those induced by fast voltage-dependent gating and relates them to the deformation of the filter region (Gazzarrini et al., 2006). Single-channel measurements presented here corroborate the existence of such a fast mechanism because at extreme voltages, the channel openings become exceedingly noisy because of unresolved closures. This is verified by the analysis of β distributions, which also allows the evaluation of the rate constants of this mechanism.

Fast gating

Fast-gating analysis of Kcv single-channel currents reveals that flickering is the reason for the negative slope in I-V curve as in MaxiK.

The common feature between Kcv and MaxiK is the increase of the gating factor I_{true}/I_{app} at high positive membrane potentials. Furthermore, the increase of k_{OC} (destabilization of the open state) is the major source of flickering. This would suggest the involvement of basically the same mechanism for the stability of the open state (described by k_{OC}). Schroeder and Hansen (2007) have suggested that fast gating at high positive membrane potentials in MaxiK results from ion depletion in the selectivity filter when voltage pulls ions more rapidly out of the filter than they can be supplemented from the cytosol. Our finding that high K^+ reduces the open-channel noise (Fig. 7 C) and increases the apparent current and conductance in Kcv (Figs. 6, A and B, and 7, A and B) also confirms for this channel a depletion-aggravated instability of the filter region. The similarities in the behavior of these two kinds of quite different channels (MaxiK and Kcv) may imply that the selectivity filter behaves quite similar in all K^+ channels, and that Kcv is a good model of K^+ channels, at least with respect to the selectivity filter. Nevertheless, there are remarkable differences between MaxiK and Kcv. Fig. 5 C shows that

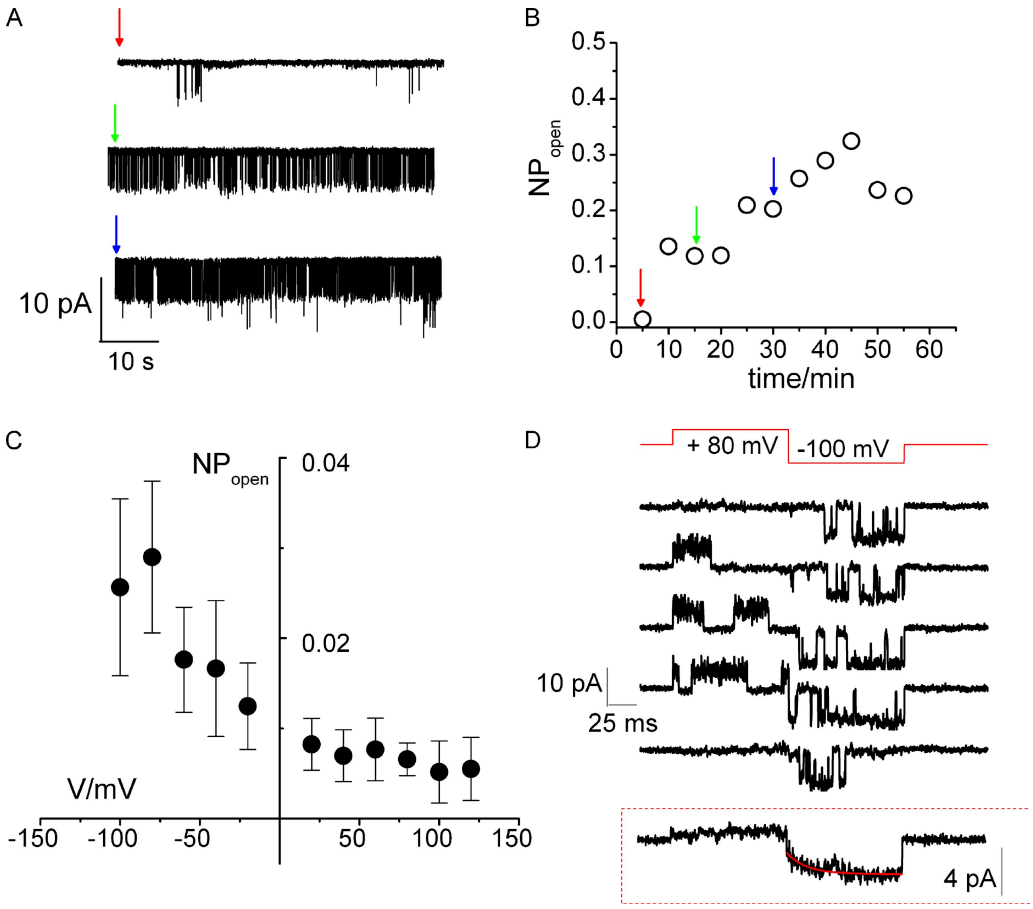

Figure 8. Open probability in Kcv. (A) Time-dependent open probability in a 60-min-long multichannel record. 1-min extract is shown from three periods of different channel activity, cross-referenced by colored arrows in B. (B) NP_{open} calculated over 5-min-long periods increases with time (the nominal open probability is T_o/T_o+T_C, independently from the number of open levels). (C) Steady-state open probability: voltage dependence obtained from records of 1 min ($n = 7$ patches). (D) Consecutive traces at +80 and −100 mV and ensemble average of 100 similar traces (boxed). Activation kinetic is fitted (red line) by a single exponential ($\tau = 17$ ms).

the increase of the gating factor at positive potentials is much stronger in Kcv than it is in MaxiK. Higher gating factors are also found in Kcv at negative potentials as a consequence of the parabolic behavior of *koc*. This is in agreement with the sporadic observation of marked flickering also at negative voltage values in Kcv (Fig. 3, right) and supports the view that the filter in Kcv is less stable than it is in MaxiK.

This gives rise to the question of why Kcv is more instable than MaxiK. A speculation may be initiated by another question; namely, why do some channels have >1,000 residues (like MaxiK) and others (like Kcv) have <100? There are some obvious answers: incorporation of the voltage sensor for voltage-induced gating, or the incorporation of cytosolic binding sites for the control by messengers. However, one issue of the increase in size may also be related to functional stability. The task of Kcv is to do harm to the attacked organism (Plugge et al., 2000; Neupärtl et al., 2008). A reliably operating selectivity filter may be of minor evolutionary value.

Slow gating

Surprisingly, Kcv spends the larger part of the time in a closed conformation (Fig. 2, left). The low open probability in steady-state recordings (Fig. 8 C) is also weakly voltage dependent, another result that needs to be considered in the identification of a gate in Kcv.

After KcsA crystallization (Doyle et al., 1998), the bundle crossing between the four inner membrane domains (TM2 or S6) has been suggested as the major gate in gated potassium channels (Perozo et al., 1998, 1999; Doyle, 2004). However, the second TM domain of Kcv is 19 amino acids long and appears too short to form an efficient bundle crossing (Tayefeh et al., 2009). The small dimensions of Kcv, basically the simple pore domain, constrain us to presume an involvement of the filter region also in the slow gating of the channel. Different observations in other potassium channels support the idea of a flexible filter switching between nonconductive and conductive states. First, certain permeant ions affect gating in channels, specifically ions with higher occupancy like rubidium or thallium (Swenson and Armstrong, 1981;

Spruce et al., 1989; Shapiro and DeCoursey, 1991; Demo and Yellen, 1992, Piskorowski and Aldrich, 2006; Schroeder and Hansen, 2008). In Kcv, slow-gating kinetics is modified by external rubidium (Kang et al., 2004). Moreover, some slow-gating mechanisms are clearly associated with the filter region, such as C-type inactivation in voltage-dependent potassium channels (Kiss and Korn, 1998; Yellen, 1998). The time constant of C inactivation is by two to three orders of magnitude larger than that of the slow gating reported here. However, Vaid et al. (2008) revealed a time constant in a dequenching phase of fluorescence from TMRM-labeled Kv1.5 in the temporal range of the slow-gating effect in Kcv. By means of mutational studies, this component was assigned to conformational changes in the selectivity filter. Similarly, in KcsA upon pH activation, an inactivation mechanism is revealed. This mechanism involves hydrogen bonds between residues D80 in the selectivity filter and E71 and W67 in the adjacent pore helix (Gao et al., 2005; Blunck et al., 2006; Cordero-Morales et al., 2006, 2007). A similar combination of amino acids is also present in Kcv, with the exception of the glutamate, substituted in Kcv by a threonine. Because mutation E71T maintains the inactivation in KcsA (Cordero-Morales et al., 2007), we can speculate that a similar inactivation mechanism is also active in Kcv.

In conclusion, the voltage dependence of the fast gating is clearly related to the rate constants of the O-C model. As discussed above, the strong dependence at high membrane potentials can be explained by voltage-induced ion depletion, and it does not require a separate voltage sensor. On the contrary, the voltage dependence of the slow gating is not clear, and our attempts to relate it to the operation of a bundle crossing have so far failed. But there is some evidence that its origin is also in the selectivity filter.

This investigation was supported in part by EU FP7 project European Drug Initiative on Channels and Transporters (EDICT; grant number 201924 to A. Moroni) and by the Deutsche Forschungsgemeinschaft (grant Ha712/14-3 to U.P. Hansen).

Lawrence G. Palmer served as editor.

Submitted: 1 June 2009
Accepted: 23 July 2009

REFERENCES

Bernèche, S., and B. Roux. 2005. A gate in the selectivity filter of potassium channels. *Structure.* 13:591–600.

Blunck, R., J.F. Cordero-Morales, L.G. Cuello, E. Perozo, and F. Bezanilla. 2006. Detection of the opening of the bundle crossing in KcsA with fluorescence lifetime spectroscopy reveals the existence of two gates for ion conduction. *J. Gen. Physiol.* 128:569–581.

Caceci, M.S., and W.P. Cacheris. 1984. Fitting curves to data—the simplex algorithm is the answer. *Byte.* 9:340–362.

Cordero-Morales, J.F., L.G. Cuello, Y. Zhao, V. Jogini, D.M. Cortes, B. Roux, and E. Perozo. 2006. Molecular determinants of gating at the potassium-channel selectivity filter. *Nat. Struct. Mol. Biol.* 13:311–318.

Cordero-Morales, J.F., V. Jogini, A. Lewis, V. Vásquez, D.M. Cortes, B. Roux, and E. Perozo. 2007. Molecular driving forces determining potassium channel slow inactivation. *Nat. Struct. Mol. Biol.* 14:1062–1069.

Demo, S.D., and G. Yellen. 1992. Ion effects on gating of the $Ca^{(2+)}$-activated K^+ channel correlate with occupancy of the pore. *Biophys. J.* 61:639–648.

Doyle, D.A. 2004. Structural changes during ion channel gating. *Trends Neurosci.* 27:298–302.

Doyle, D.A., J. Morais Cabral, R.A. Pfuetzner, A. Kuo, J.M. Gulbis, S.L. Cohen, B.T. Chait, and R. MacKinnon. 1998. The structure of the potassium channel: molecular basis of K^+ conduction and selectivity. *Science.* 280:69–77.

Draber, S., and U.P. Hansen. 1994. Fast single-channel measurements resolve the blocking effect of Cs^+ on the K^+ channel. *Biophys. J.* 67:120–129.

Fitzhugh, R. 1983. Statistical properties of the asymmetric random telegraph signal, with applications to single-channel analysis. *Math. Biosci.* 64:75–89.

Gao, L., X. Mi, V. Paajanen, K. Wang, and Z. Fan. 2005. Activation-coupled inactivation in the bacterial potassium channel KcsA. *Proc. Natl. Acad. Sci. USA.* 102:17630–17635.

Gazzarrini, S., J.L. Etten, D. DiFrancesco, G. Thiel, and A. Moroni. 2002. Voltage-dependence of virus-encoded miniature K^+ channel Kcv. *J. Membr. Biol.* 187:15–25.

Gazzarrini, S., A. Abenavoli, D. Gradmann, G. Thiel, and A. Moroni. 2006. Electrokinetics of miniature K^+ channel: open-state *V* sensitivity and inhibition by K^+ driving force. *J. Membr. Biol.* 214:9–17.

Hansen, U.P., O. Cakan, M. Abshagen-Keunecke, and A. Farokhi. 2003. Gating models of the anomalous mole-fraction effect of single-channel current in *Chara*. *J. Membr. Biol.* 192:45–63.

Heinemann, S.H., and F.J. Sigworth. 1991. Open channel noise. VI. Analysis of amplitude histograms to determine rapid kinetic parameters. *Biophys. J.* 60:577–587.

Hille, B. 1992. Ionic Channels of Excitable Membranes. 2nd ed. Sinauer Associates, Inc., Sunderland, MA. 607 pp.

Kang, M., A. Moroni, S. Gazzarrini, D. DiFrancesco, G. Thiel, M. Severino, and J.L. Van Etten. 2004. Small potassium ion channel proteins encoded by chlorella viruses. *Proc. Natl. Acad. Sci. USA.* 101:5318–5324.

Kiss, L., and S.J. Korn. 1998. Modulation of C-type inactivation by K^+ at the potassium channel selectivity filter. *Biophys. J.* 74:1840–1849.

Klieber, H.G., and D. Gradmann. 1993. Enzyme kinetics of the prime K^+ channel in the tonoplast of *Chara*: selectivity and inhibition. *J. Membr. Biol.* 132:253–265.

Kuo, A., J.M. Gulbis, J.F. Antcliff, T. Rahman, E.D. Lowe, J. Zimmer, J. Cuthbertson, F.M. Ashcroft, T. Ezaki, and D.A. Doyle. 2003. Crystal structure of the potassium channel KirBac1.1 in the closed state. *Science.* 300:1922–1926.

Liu, Y., M.E. Jurman, and G. Yellen. 1996. Dynamic rearrangement of the outer mouth of a K+ channel during gating. *Neuron.* 16:859–867.

Moroni, A., C. Viscomi, V. Sangiorgio, C. Pagliuca, T. Meckel, F. Horvath, S. Gazzarrini, P. Valbuzzi, J.L. Van Etten, D. DiFrancesco, and G. Thiel. 2002. The short N-terminus is required for functional expression of the virus-encoded miniature K(+) channel Kcv. *FEBS Lett.* 530:65–69.

Neupärtl, M., C. Meyer, I. Woll, F. Frohns, M. Kang, J.L. Van Etten, D. Kramer, B. Hertel, A. Moroni, and G. Thiel. 2008. Chlorella viruses evoke a rapid release of K+ from host cells during the early phase of infection. *Virology.* 372:340–348.

Pagliuca, C., T.A. Goetze, R. Wagner, G. Thiel, A. Moroni, and D. Parcej. 2007. Molecular properties of Kcv, a virus encoded K^+ channel. *Biochemistry.* 46:1079–1090.

Perozo, E., D.M. Cortes, and L.G. Cuello. 1998. Three-dimensional architecture and gating mechanism of a K+ channel studied by EPR spectroscopy. *Nat. Struct. Biol.* 5:459–469.

Perozo, E., D.M. Cortes, and L.G. Cuello. 1999. Structural rearrangements underlying K+-channel activation gating. *Science.* 285:73–78.

Piskorowski, R.A., and R.W. Aldrich. 2006. Relationship between pore occupancy and gating in BK potassium channels. *J. Gen. Physiol.* 127:557–576.

Plugge, B., S. Gazzarrini, M. Nelson, R. Cerana, J.L. Van Etten, C. Derst, D. DiFrancesco, A. Moroni, and G. Thiel. 2000. A potassium channel protein encoded by chlorella virus PBCV-1. *Science.* 287:1641–1644.

Riessner, T. 1998. Level detection and extended Beta distributions for the analysis of fast rate constants of Markov processes in sampled data. PhD thesis. Aachen University, Aachen, Germany. 74 pp.

Schröder, I., T. Huth, V. Suitchmezian, J. Jarosik, S. Schnell, and U.P. Hansen. 2004. Distributions-per-level: a means of testing level detectors and models of patch-clamp data. *J. Membr. Biol.* 197:49–58.

Schroeder, I., and U.P. Hansen. 2006. Strengths and limits of Beta distributions as a means of reconstructing the true single-channel current in patch clamp time series with fast gating. *J. Membr. Biol.* 210:199–212.

Schroeder, I., and U.P. Hansen. 2007. Saturation and microsecond gating of current indicate depletion-induced instability of the MaxiK selectivity filter. *J. Gen. Physiol.* 130:83–97.

Schroeder, I., and U.P. Hansen. 2008. Tl^+-induced μs gating of current indicates instability of the MaxiK selectivity filter as caused by ion/pore interaction. *J. Gen. Physiol.* 131:365–378.

Schultze, R., and S. Draber. 1993. A nonlinear filter algorithm for the detection of jumps in patch-clamp data. *J. Membr. Biol.* 132:41–52.

Shapiro, M.S., and T.E. DeCoursey. 1991. Selectivity and gating of the type L potassium channel in mouse lymphocytes. *J. Gen. Physiol.* 97:1227–1250.

Shim, J.W., M. Yang, and L.Q. Gu. 2007. In vitro synthesis, tetramerization and single channel characterization of virus-encoded potassium channel Kcv. *FEBS Lett.* 581:1027–1034.

Sigworth, F.J. 1985. Open channel noise. I. Noise in acetylcholine receptor currents suggests conformational fluctuations. *Biophys. J.* 47:709–720.

Spruce, A.E., N.B. Standen, and P.R. Stanfield. 1989. Rubidium ions and the gating of delayed rectifier potassium channels of frog skeletal muscle. *J. Physiol.* 411:597–610.

Swenson, R.P., Jr., and C.M. Armstrong. 1981. K^+ channels close more slowly in the presence of external K^+ and Rb^+. *Nature.* 291:427–429.

Tayefeh, S., T. Kloss, G. Thiel, B. Hertel, A. Moroni, and S.M. Kast. 2007. Molecular dynamics simulation of the cytosolic mouth in Kcv-type potassium channels. *Biochemistry.* 46:4826–4839.

Tayefeh, S., T. Kloss, M. Kreim, M. Gebhardt, D. Baumeister, B. Hertel, C. Richter, H. Schwalbe, A. Moroni, G. Thiel, and S.M. Kast. 2009. Model development for the viral Kcv potassium channel. *Biophys. J.* 96:485–498.

Townsend, C., and R. Horn. 1999. Interaction between the pore and a fast gate of the cardiac sodium channel. *J. Gen. Physiol.* 113:321–332.

Vaid, M., T.W. Claydon, S. Rezazadeh, and D. Fedida. 2008. Voltage clamp fluorimetry reveals a novel outer pore instability in a mammalian voltage-gated potassium channel. *J. Gen. Physiol.* 132:209–222.

VanDongen, A.M. 2004. K channel gating by an affinity-switching selectivity filter. *Proc. Natl. Acad. Sci. USA.* 101:3248–3252.

Weber, W.M. 1999. Ion currents of *Xenopus laevis* oocytes: state of the art. *Biochim. Biophys. Acta.* 1421:213–233.

Weise, R., and D. Gradmann. 2000. Effects of Na(+) on the predominant K(+) channel in the tonoplast of Chara: decrease of conductance by blocks in 100 nanosecond range and induction of oligo- or poly-subconductance gating modes. *J. Membr. Biol.* 175:87–93.

Yellen, G. 1984. Ionic permeation and blockade in Ca^{2+}-activated K^+ channels of bovine chromaffin cells. *J. Gen. Physiol.* 84:157–186.

Yellen, G. 1998. The moving parts of voltage-gated ion channels. *Q. Rev. Biophys.* 31:239–295.